JOURNAL OF MECHANICS OF CONTINUA AND MATHEMATICAL SCIENCES
www.journalimcms.org

ISSN (Online) : 2454 -7190 Vol.-15, No.-7, July (2020) pp 99-116 ISSN (Print) 0973-8975

ELECTROMAGNETIC EFFECT ON FREE FLOW OF THE NANOFLUID IN ABSORBER OF CONCENTRATED SOLAR COLLECTOR

Dheyaa A. Khalaf[1], Karima E. Amori[2], Firas M.Tuaimah[3]

[1]Department of Mechanical Engineering, College of Engineering, University of Baghdad, Iraq.

[2]Professor, Department of Mechanical Engineering, College of Engineering, University of Baghdad, Iraq.

[3]Professor, Department of Electrical Engineering, College of Engineering, University of Baghdad, Iraq.

[1]Deyaaaliqabi@gmail.com, [2]drkarimaa63@gmail.com, [3]dr.firasmt@gmail.com

Corresponding Author: Dheyaa A. Khalaf

https://doi.org/10.26782/jmcms.2020.07.00008

Abstract

In this work, the effect of electromagnetic field on natural fluid flow within the absorbent tube in the parabolic solar collector was numerical investigated. Where a solar collector with parabolic reflector was used.

Water was used in the first and the flow was free as the results showed high efficiency of the device. Then a magnetic iron oxide (Fe_3O_4) nanoparticle was added to make the fluid subject to influence in the electromagnetic field, where three concentrations (0.9%, 0.5%, and 0.3%) were used to study the effect of magnetic flux on each concentration and to make a comparison.

The results showed a slight effect of the electromagnetic field in the case of water use, as the efficiency of the solar collector improved by (8.8%) in the case of using the concentration (0.9%) and an electromagnetic overflow (7970 Gauss).

Keywords : Magnetic field, Nanofluid, Nanofluid Properties, Ferrfluid, Nano Particles, Solar energy, solar collector, heat transfer enhancement

I. Introduction

Renewable energies are advised to supply a arrangement to eliminate dispose of the worldwide warming issue and lighten the potential of vitality emergency. The request of fossil powers will be detracted when the renewable energies gotten to be accessible in vitality advertise with acceptable cost and easy technology. Besides,

potential climate alter will be reduced when the renewable energies **(Tyagiet al. 2012).**

Solar collectors are converts the energy of solar radiation to the inside vitality of the transport medium. Solar collectors are currently considered to be an important source of energy due to the availability of alternative energy.
The energy absorbed from solar radiation in solar collectors is limited by the working fluid absorption properties. Use nanofluids instead of conventional fluids is found as a potential area where the performance of solar collectors can be improved. For energy applications, a noticeable privilege of nanofluidis obtained, that is enhancement of heat transfer due to its thermo-physical properties **(Nagarajan et al. 2014).** One useful enhancement method for convective heat exchange is the utilization of magnetic field. Where liquid encounters a Lorentz force that influences the rate of mass and heat transfer. The ponder of an electrically conducting liquid in building applications is of considerable intrigued, particularly in metallurgical and metalworking forms or within the division of liquid metals from non-metallic incorporations by the application of a electromagnetic field.

(Aminfar et al. 2012) investigated numerically of the hydro-thermal behavior of a ferrofluid (4 vol% Fe_3O_4/seawater).Three situations for the magnetic field have been treated to ponder blended the ferrofluid convection: uniform transverse field, non-uniform pivotal field (positive and negative gradient) and another situation when both areas are connected at the same time. **(Mohsen et al. 2014)** examined numerically effect of magnetic-field on nanofluids (CuO-water) flow and natural convective heat-transfer in an enclosure which from below heated. Lattice-Boltzmann-method is applied to solve the governing equations. The results uncover that upgrade in heat transfer increments as Hartman-number and warm source length increment but it diminishes with increment of Rayleighs-number. **(Sheikhzadeh et al. 2012)** investigated numerically the blended convection in a differentially thermal lid-driven square depression filled with nanofluid (Cu/water) beneath the impact of a attractive field. The right and left dividers of the depression are kept at temperatures Tc and Thindividually whereas the level dividers are adiabatic. **(Hussein et al. 2014)** Numerically study of magneto-hydrodynamic free convection flow of nanofluid (Cu-water) in an open enclosure utilizing the lattice Boltzmann method (LBM). Results demonstrate that supreme values of stream work are declined altogether by expanding Hartmann-numbers whereas these values raised by expanding Rayleighs-numbers.

In this study, the theoretical side and the governing equations for fluid flow inside the absorbent tube in the solar collector under the influence of electromagnetic overflow will be reviewed. On the other hand, about numerical analysis CFD package ANSYS (CFX) software has been used to supported and compare experimental results.

II. Mathematical Model

Fluid flow governing equations under the influence of the electromagnetic field and the boundary conditions used in the numerical model is addressed. Figure (1) shows a cylindrical coordinate.

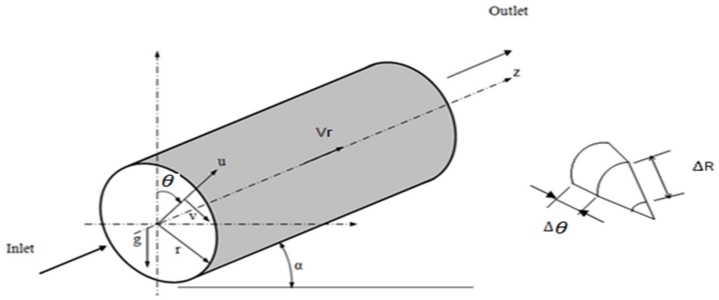

Fig. 1: Cylindrical Coordinate for Solar Collector Absorber Tube

II.i. Governing Equations

Equations can be classified into three classes; electromagnetic system, a thermal system, and fluid dynamic system.

Under the assumptions stated above, the flow field is governed by the equations

(i) Electromagnetic System

The electromagnetic framework comprises: the Gauss law, attractive acceptance condition alongside Ohm's law and Poisson's condition. These conditions characterize the dispersion of the attractive flux thickness, the electric field, and the current-thickness add up to attractive field is the entirety of the connected and initiated attractive areas. The relative quality of the actuated field is overwhelmingly characterized by a dimensionless number; the attractive Reynolds number. The magnetic field components are given as:

$$\nabla . D = \rho c \text{(Gauss law)} \quad (1)$$

$$\nabla . B = 0 \text{(No magnetic monopoles)} \quad (2)$$

$$\frac{\partial B}{\partial t} = \frac{1}{\sigma_e \mu} \nabla^2 B \quad \text{(Magnetic Induction)} \quad (3)$$

$$Re_m, = \sigma_e \mu_m UL \quad \text{(magnetic Reynolds number)} \quad (4)$$

The electrical field components are given as:

$$\nabla^2 \emptyset_e = \nabla . (U \times B) \quad \text{(Poisson's Equation)} \quad (5)$$

$$\nabla \times H = \frac{\partial D}{\partial t} + J \quad \text{(Ampere law)} \quad (6)$$

$$J = \sigma_e \text{ (E + U x B)} \quad \text{(Ohm's Law)} \quad (7)$$

$$\nabla \times E = -\frac{\partial D}{\partial t} \quad \text{(Faraday law)} \quad (8)$$

$$E = -\nabla \emptyset_e \quad (9)$$

Where;

ρ_c : electric charge density (C/m^3)

D: electric displacement (C/m^2)

B: magnetic-flux density (kg /A.s^2) (Tesla)

H: magnetic-field intensity (A/m)

E: electric-field intensity (N/C)

J: electric-current density (A/m^2)

$\emptyset_e$: electric potential (J/C)

Lorentz force (F) is defined as:

$$F = J \times B \tag{10}$$

(ii) Fluid Dynamics System

It is consist of Navier–Stokes equation and Continuity equation.

continuity-equation:

$$\frac{\partial \rho}{\partial t} + \frac{1}{r}\frac{\partial}{\partial r}(\rho r v_r) + \frac{1}{r}\frac{\partial}{\partial \theta}(\rho v_\theta) + \frac{\partial}{\partial z}(\rho v_z) = 0 \tag{11}$$

Navier–Stokes equation:

r component

$$\frac{\partial}{\partial t}(v_r) + v_r\frac{\partial v_r}{\partial r} + \frac{v_\theta}{r}\frac{\partial v_r}{\partial \theta} - \frac{v_\theta^2}{r} + v_z\frac{\partial v_r}{\partial z} = -\frac{1}{\rho_{nf}}\frac{\partial P}{\partial r} + \frac{\mu_{nf}}{\rho_{nf}}\left(\frac{\partial}{\partial r}\left(\frac{1}{r}\frac{\partial}{\partial r}(r v_r)\right) + \frac{1}{r^2}\frac{\partial^2 v_r}{\partial \theta^2} - \frac{2}{r^2}\frac{\partial v_\theta}{\partial \theta} + \frac{\partial^2 v_r}{\partial z^2}\right) + g(cos\theta cos\alpha) + f_r \tag{12}$$

Where μ_{nf},ρ_{nf} are the dynamic viscosity and the density of nanofluid in the buoyancy term, respectively, and ρ_{nf} is given by, **(Kumar and Mullick 2015).**

$$\rho_{nf}=(1-\Phi)\,\rho_f+\Phi\rho_s \tag{13}$$

Where: ρ_f,ρ_s are the densities of (fluid & solid), respectively

θ component

$$\frac{\partial}{\partial t}(v_\theta) + v_r\frac{\partial v_\theta}{\partial r} + \frac{v_\theta}{r}\frac{\partial v_\theta}{\partial \theta} - \frac{v_r v_\theta}{r} + v_z\frac{\partial v_\theta}{\partial z} = -\frac{1}{\rho_{nf}}\frac{\partial P}{r\partial \theta} + \frac{\mu_{nf}}{\rho_{nf}}\left(\frac{\partial}{\partial r}\left(\frac{1}{r}\frac{\partial}{\partial r}(r v_\theta)\right) + \frac{1}{r^2}\frac{\partial^2 v_\theta}{\partial \theta^2} + \frac{2}{r^2}\frac{\partial v_\theta}{\partial \theta} + \frac{2}{r^2}\frac{\partial^2 v_\theta}{\partial z^2}\right) + g(\sin\theta\cos\alpha) + f_\theta \tag{14}$$

z component

$$\frac{\partial}{\partial t}(v_z) + v_r\frac{\partial v_z}{\partial r} + \frac{v_\theta}{r}\frac{\partial v_z}{\partial \theta} + v_z\frac{\partial v_z}{\partial z} = -\frac{1}{\rho_{nf}}\frac{\partial P}{\partial z} + \frac{\mu_{nf}}{\rho_{nf}}\left(\frac{1}{r}\frac{\partial}{\partial r}\left(r\frac{\partial v_z}{\partial r}\right) + \frac{1}{r^2}\frac{\partial^2 v_z}{\partial \theta^2} + \frac{\partial^2 v_z}{\partial z^2}\right) + g(\sin\alpha) + f_z \tag{15}$$

Where

v_r , v_θ *and* v_z: velocity components.

ρ_{nf}: nanofluid density (constant)

μ_{nf} : dynamic viscosity of the nanofluid (constant)

f denote the components of the body forces per unit volume.

(iii) Thermal System

The energy equation of incompressible fluid describes the relationship between the velocity field and the thermal field, integrated with electric-magnetic field is defined as:

$$\frac{\partial T}{\partial t}+v_r\frac{\partial T}{\partial r}+\frac{v_\theta}{r}\frac{\partial T}{\partial \theta}+v_z\frac{\partial T}{\partial z}=\frac{k_{nf}}{\rho cp}\left\{\frac{1}{r}\frac{\partial}{\partial r}\left(r\frac{\partial T}{\partial r}\right)+\frac{1}{r^2}\frac{\partial^2 T}{\partial \theta^2}+\frac{\partial^2 T}{\partial z^2}\right\}$$

$$+\frac{|J|^2}{\sigma_e} \tag{16}$$

Effective Thermal Conductivity (Abu-Nada 2008);

$$k_{nf}=\left[\frac{k_s+(n-1)k_f-(n-1)\Phi(k_f-k_s)}{k_s+(n-1)k_f+\Phi(k_f-k_s)}\right]k_f \tag{17}$$

Where: n is a shape factor and equals to 3 for spherical nanoparticles.

Thermal Diffusivity (Zhang 2007);

$$\alpha_{nf}=\frac{k_{nf}}{(1-\Phi)(\rho cp)_f+\Phi(\rho cp)_s} \tag{18}$$

Thermal Expansion Coefficient (Titan 2013);

$$\beta_{nf}=\left[\frac{1}{1+\frac{(1-\Phi)\rho_f}{\Phi\rho_s}\frac{\beta_s}{\beta_f}}+\frac{1}{1+\frac{\Phi}{1-\Phi}\frac{\rho_s}{\rho_f}}\right]\beta_f \tag{19}$$

Specific Heat (Titan 2013);

$$cp_{nf}=\left[\frac{(1-\Phi)(\rho cp)_f+\Phi(\rho cp)_s}{(1-\Phi)\rho_f+\Phi\rho_s}\right] \tag{20}$$

Effective Viscosity (Maiga2006);

$$\mu_{nf}=[123\Phi^2+7.3\Phi+1] \tag{21}$$

Φ Volume fraction

II.i. Thermal Analysis

As the working fluid in the receiver absorbs energy, its temperature will increase. This increase a temperature difference between the temperature of the fluid, absorber, glass cover and the temperature of the ambient air. Heat losses from the absorber tube to the glass cover surface and from the glass cover surface to ambient air are driven by this temperature difference.

The useful energy is calculated by the following equation.

$$Q_u=A_cF_R[I_s-U_L\frac{A_{tube}}{A_g}(T_i-T_{amb})] \tag{22}$$

Where

A_c: Collector area.

I_s: Solar beam radiation intensity (W/m^2).

T_i: Inlet fluid temperature (K).

T_{amb} : Ambient temperature(K).

F_R: Heat removal factor is calculated by:

$$F_R = \frac{\dot{m}\, cp}{A_c U_L}\left[1 - e^{-\left(\frac{A_c U_L \grave{F}}{\dot{m}\, cp}\right)}\right] \quad (23)$$

U_L: Collector heat loss coefficient is calculated by:

$$U_L = \left[\frac{A_{tube}}{A_g\, h_{r,g}} + \frac{1}{h_{g,tube}}\right]^{-1} \quad (24)$$

Where

hr,g: Heat-transfer coefficient due to radiation between the glass cover surface and ambient air (W/m^2.K). It is calculated as

$$hr,g = \varepsilon_g \sigma (T_g + T_{sky})(T_g^{\,2} + T_{sky}^{\,2}) \quad (25)$$

$$T_{sky} = \varepsilon_{sky}^{\frac{1}{4}} T_{amb}^{\,2} \quad (26)$$

$h_{r,g\text{-}amb}$: Radiation Heat-transfer coefficient between the absorber tube and glass cover surface (W/m^2.K). It is calculated as **(Duffie1974)**:

$$h_{tube,g} = \frac{\sigma(T_{tube} + T_g)(T_{tube}^{\,2} + T_g^{\,2})}{\frac{1}{\varepsilon_{tube}} + \frac{A_{tube}}{A_g}\left(\frac{1}{\varepsilon_g} - 1\right)} \quad (27)$$

Where:

A_g: Area of glass covers.

ε_g: Emissivity of the glass covers (0.94).

ε_{abs}: Emissivity of the absorber metal (0.88).

σ: Stefan-Boltzmann constant which 5.67×10^{-8} W/m^2 .K^4.

T_g: Temperature of the glass cover (K).

T_{tube}: Absorber tube temperature (K).

k_{abs} are the thermal conductivity of the absorber metal (W/m.K), and $D_{abs,o}$is outside diameter of the absorber (0.014m).

The collector efficiency factor (F′) is the ratio between actual useful energy collected to the useful energy collected and calculated as:

$$\grave{F} = \frac{1/U_L}{\frac{1}{U_L} + \frac{D_o}{h_{fi} D_i} + \frac{D_o}{2K} ln\frac{D_o}{D_i}} \quad (28)$$

Where

h_{fi}: convection heat-transfer of fluid flow inside absorber tube, to calculate its value, the type of flow is determined after the value of Grashof 's number, If the value of the $Gr < 10^9$, then this means that the flow is laminar and the calculation of the nusselt number is according to the following equation

$$Nu = 0.677\ P_r{}^{0.5}(0.95\ P_r)^{-.025} Gr^{0.25} \tag{29}$$

Then;

$$h_{fi} = \frac{NuK_f}{D_i} \tag{30}$$

III. Numerical Solution

The numerical analysis will be reviewed, regarding (System Geometry, Grid Generation, Size Function and Number of Iterations and Convergence Criteria) using a program ANSYS (CFX).

It is a high performance, general object CFD program that has been applied to solve wide ranging fluid flow problems. ANSYS CFX is its advanced solver technology, the key to achieving reliable and accurate solutions quickly and robustly.

In this study used coupled algorithm, using the coupled path offers some advantages over the non-coupled or separated approach. Also it is using for transient flows, it is necessary when the quality of the mesh is poor, or used large time steps are.

III.i. System Geometry

The system Geometry consists of a copper absorber tube of (12.4 mm) ID, (0.6mm) thickness and (2200 mm) in length. Where the fluid flow is in the tube natural and the magnetic flux is projected in addition to the solar radiation. Shown in figure (2).

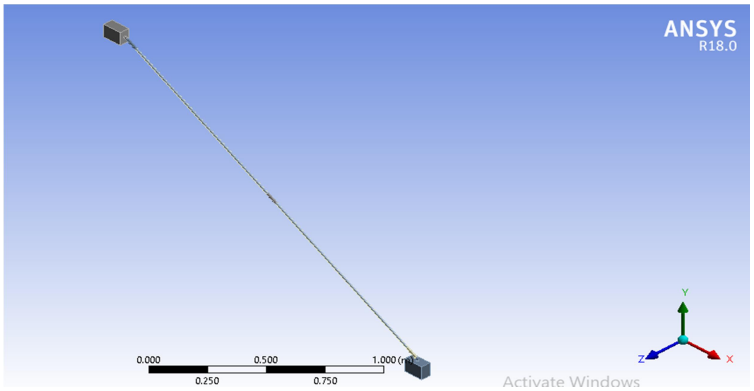

Fig. 2: System Geometry

III.ii. Grid Generation and Size Function

Once the governing equations have been discredited, appropriate grid needs to be generated to exemplify the nodes and/or cells by the computational domain. Unstructured grids are in general successful for complex geometries, so for the above reason, the unstructured tetrahedron grids are used in the current study. The number of mesh elements in this study is (970,046) and nodes (1,695,208) shown in figure (3).

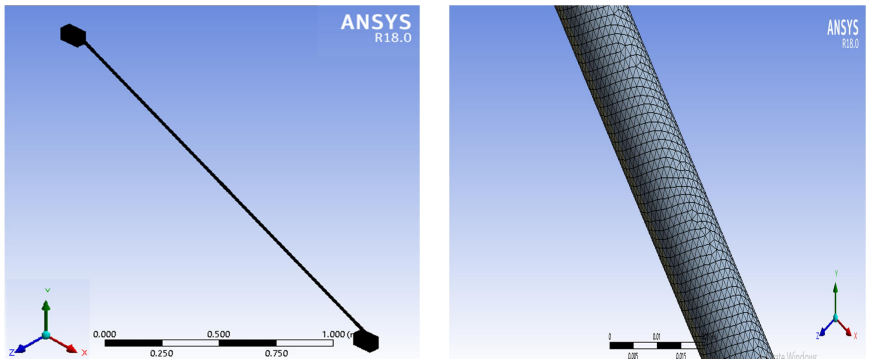

(a) (b)

Fig. 3.3: Grid of System Geometry.(a)The Overall Shape, (b)Close-Up Image

The three sizing jobs (fixed, proximity, and curvature) are used to control the size of mesh entr'acte for edges and mesh elements for faces or volumes. Fixed and curvature are the most commonly used. The specifications (type, entities, and parameters) must be defined. The size function parameters define the exact characteristics of the size function. The type specification determines the algorithm used by the size function to control the mesh-element edge size.

III.iii. Number of Iterations and Convergence Criteria

It is the maximum number of iterations completed before the solver terminates. For a transient simulation, the number of iterations per time steps indicates how many times the flow equations will be solved per time step before moving on to the next time step. Generally, this number is 20. You may increase or decrease this number depending on your application. Can be seen figure (4).

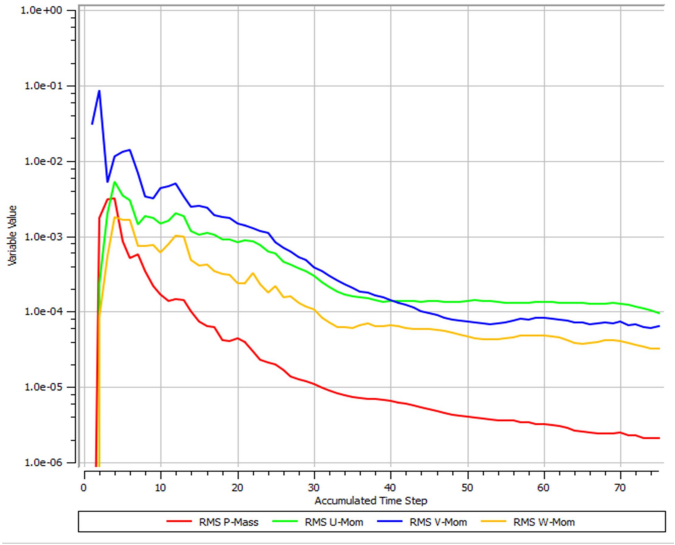

Fig. 4: Iterations and Convergence Criteria.

The color plots different show the convergence rate of each solved equation, all these tools help the user to readily recognize the Convergence of simulation is accomplished after several time steps.

IV. Results

The problem was analyzed numerically under five different volume fractions of (0, 0.3, 0.5, 0.9)% of nanoparticles (Fe_3o_4), as well as five different electromagnetic intensity of (0, 3240, 4320,6233 and 7970Gauss). Numerical results were carried out employing the finite volume method by commercial CFD (ANSYS/CFX) software.

IV.i. Working Fluid Temperature

A. Based Fluid (Water)

Figure (5) shows the temperature distribution for the water inside the absorber tube, not subjected to electromagnetic field. It is noticed that the value of the fluid temperature begins with a small value at 9:00 AM and then begins gradual increase to reach its highest value (68.2 $^{\circ}$ C) at 13:00 PM then decreases to vanish at sun set.

Figure (6) Appears the temperature distribution for the water inside the absorber tube, subjected to electromagnetic field(3240 Gauss).The maximum recorder value is (72.6 ^{o}C) at 13:00 PM .

B. Ferrofluid

Figure (7) show the temperature distribution for ferrofluid of volume concentrations of (0.3%) no subjected to electromagnetic field. The temperature at the beginning test day is low, and then rises gradually to its highest value.

Figure (8) evidence the temperature distribution for ferrofluid of volume concentrations of (0.3%) .As it gradually increases to reach the highest value (84^{o} C) at 14:00 PM when electromagnetic field 3240 Gauss and then begins to descend.

VI.ii. Working Fluid Velocity

A. Based Fluid (Water)

Figure (9) Appears the velocity distribution for the water inside the absorber tube, not subjected to electromagnetic field. It is noticed that the value of the fluid velocity begins with a small value at 9:00 AM and then begins gradual increase to reach its highest value at 13:00 PM then decreases to vanish at sun set.

Figure (10) shows the velocity distribution for the water inside the absorber tube, subjected to electromagnetic field (3240 Gauss). The maximum recorder value is (0.0086 m/s) at 13:00 PM.

B. Ferrofluid

Figure (11) show the velocity distribution for ferrofluid of volume concentrations of (0.3%) no subjected to electromagnetic field. The velocity at the beginning test day is low, then rises gradually to its highest value.

Figure (12) evidence the velocity distribution for ferrofluid of volume concentrations of (0.3%) .As it gradually increases to reach the highest value at 14:00 PM when electromagnetic field 3240 Gauss and then begins to descend.

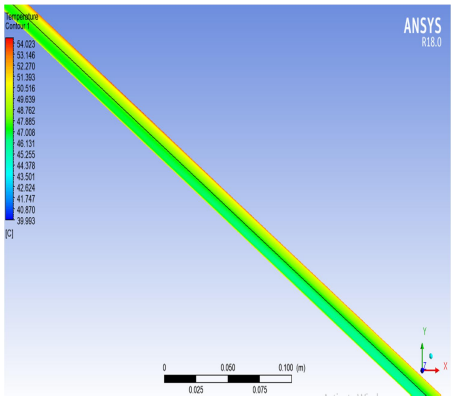

(a)

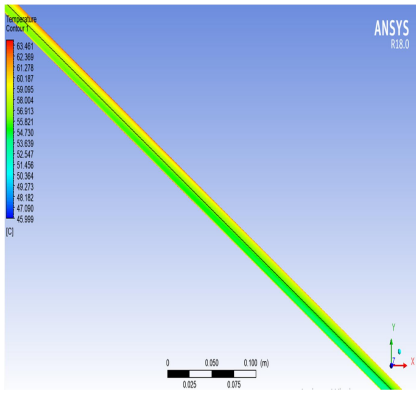

(b)

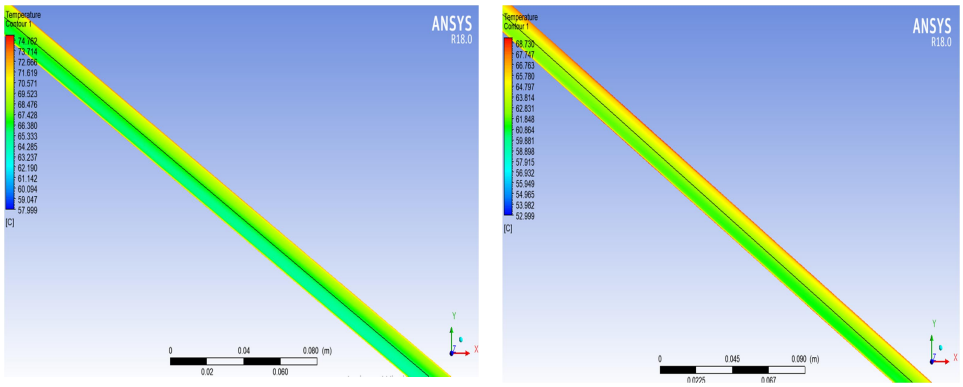

Fig. 5: Water Temperature Distribution Along the Absorber not Subjected to Electromagnetic Field a)9:00 AM b)11:00 AM c)13:00 PM d)15:00 PM.

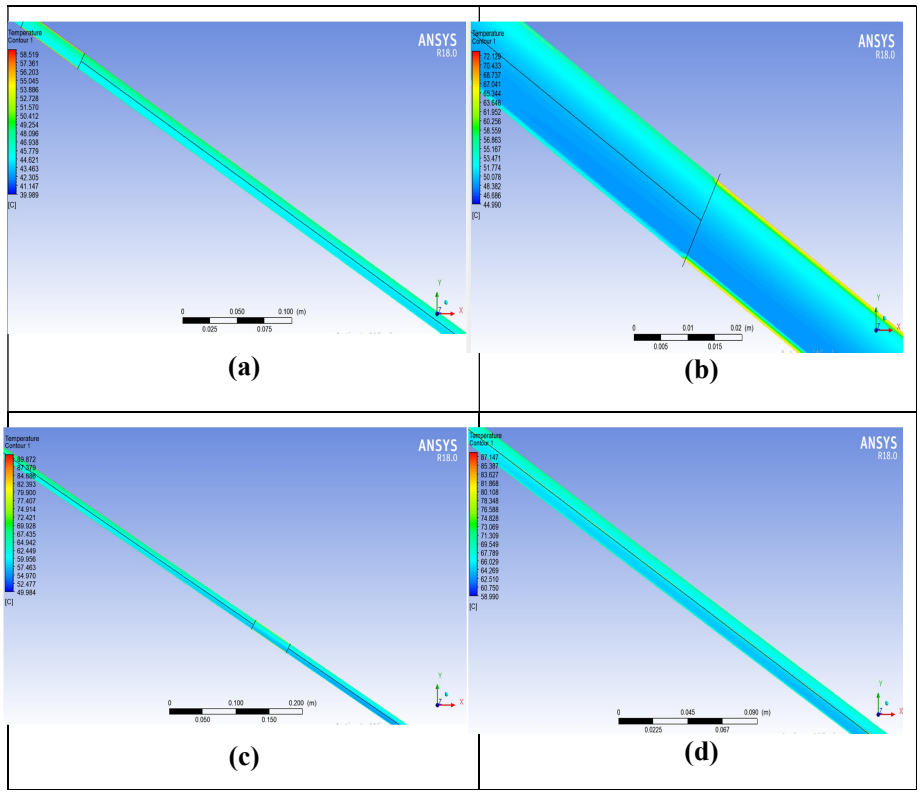

Fig. 6: Water Temperature Distribution Along the Absorber Subjected to Electromagnetic Field3240 Gauss a)9:00 Am b)11:00 AM c)13:00 PM d)15:00 PM.

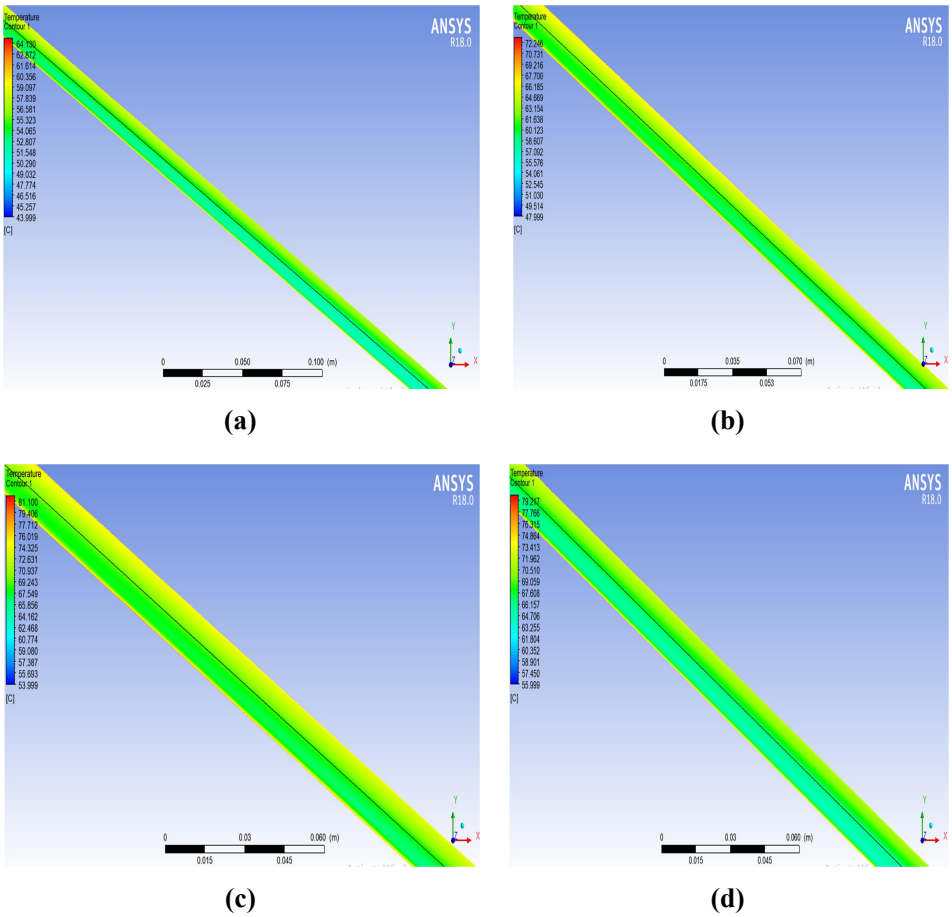

Fig. 7: Ferrofluid (φ =0.3%) Temperature Distribution Along the Absorber Subjected to Electromagnetic Field 7970 Gauss a) 9:00 Am b) 11:00 AM c) 13:00 PM d)15:00 PM.

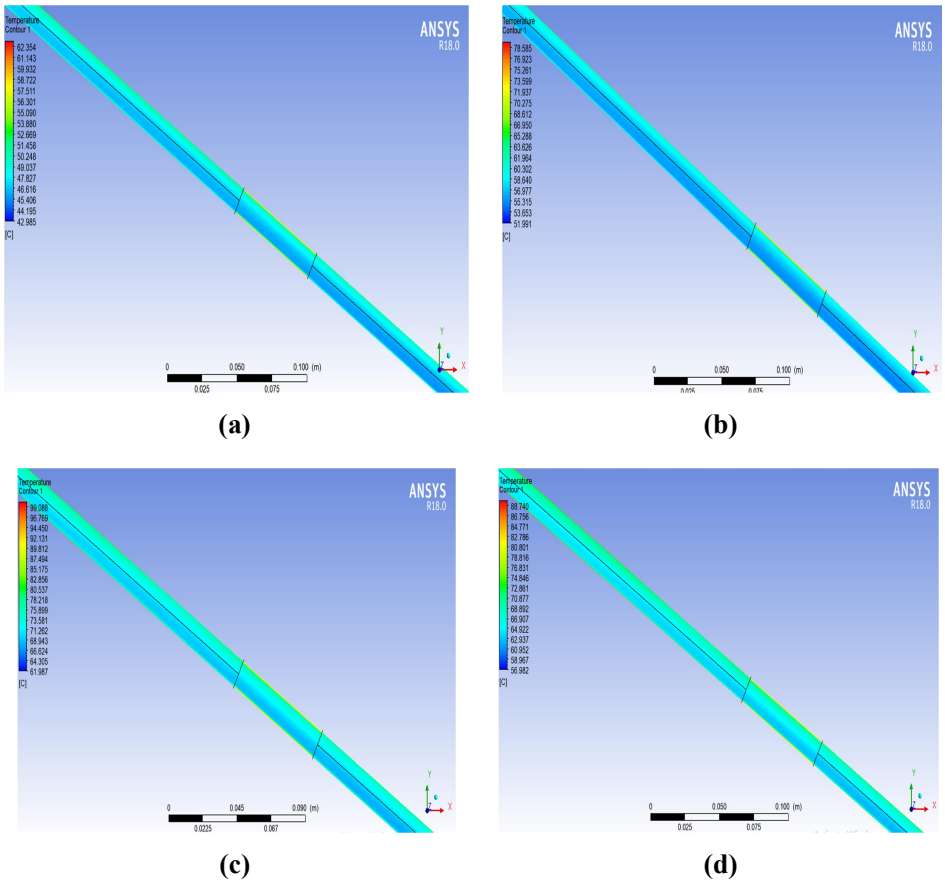

Fig. 8: Water Temperature Distribution Along the Absorber Subjected to Electromagnetic Field 7970 Gauss a) 9:00 Am b) 11:00 AM c) 13:00 PM d) 15:00 PM.

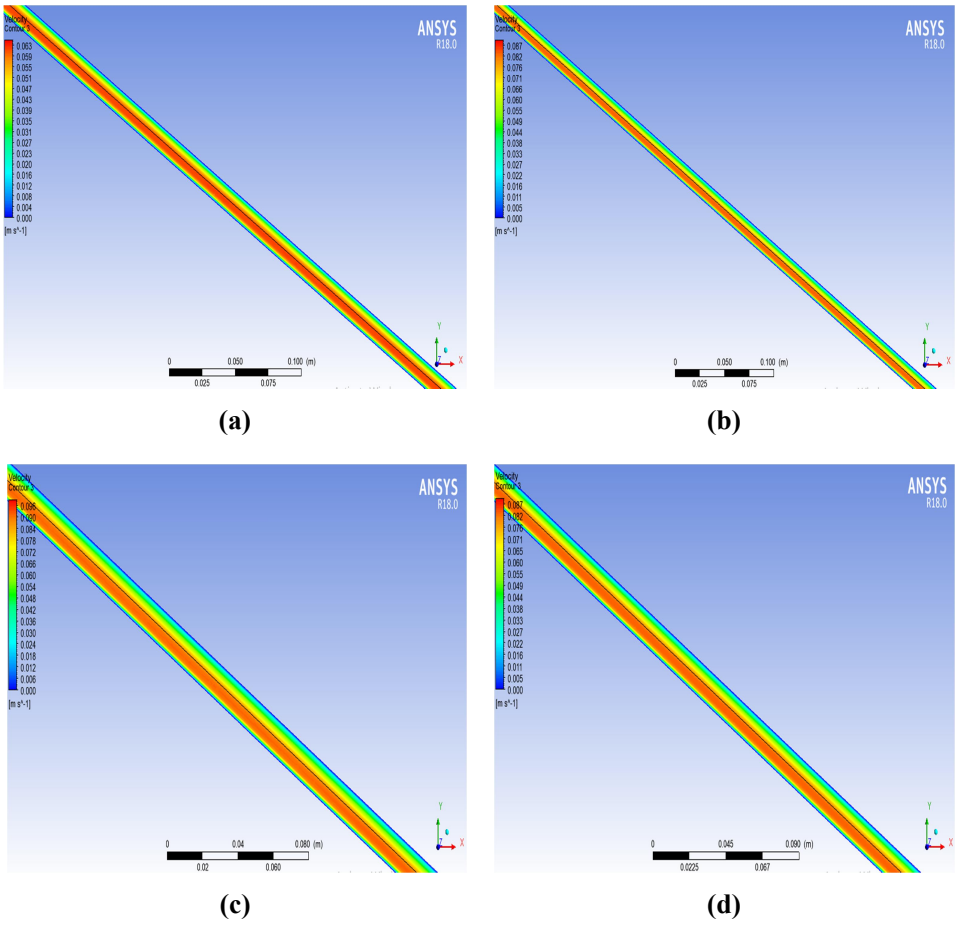

Fig. 9: Water Velocity Distribution Along the Absorber not Subjected to Electromagnetic Field a) 9:00 Am b) 11:00 AM c) 13:00 PM d) 15:00 PM.

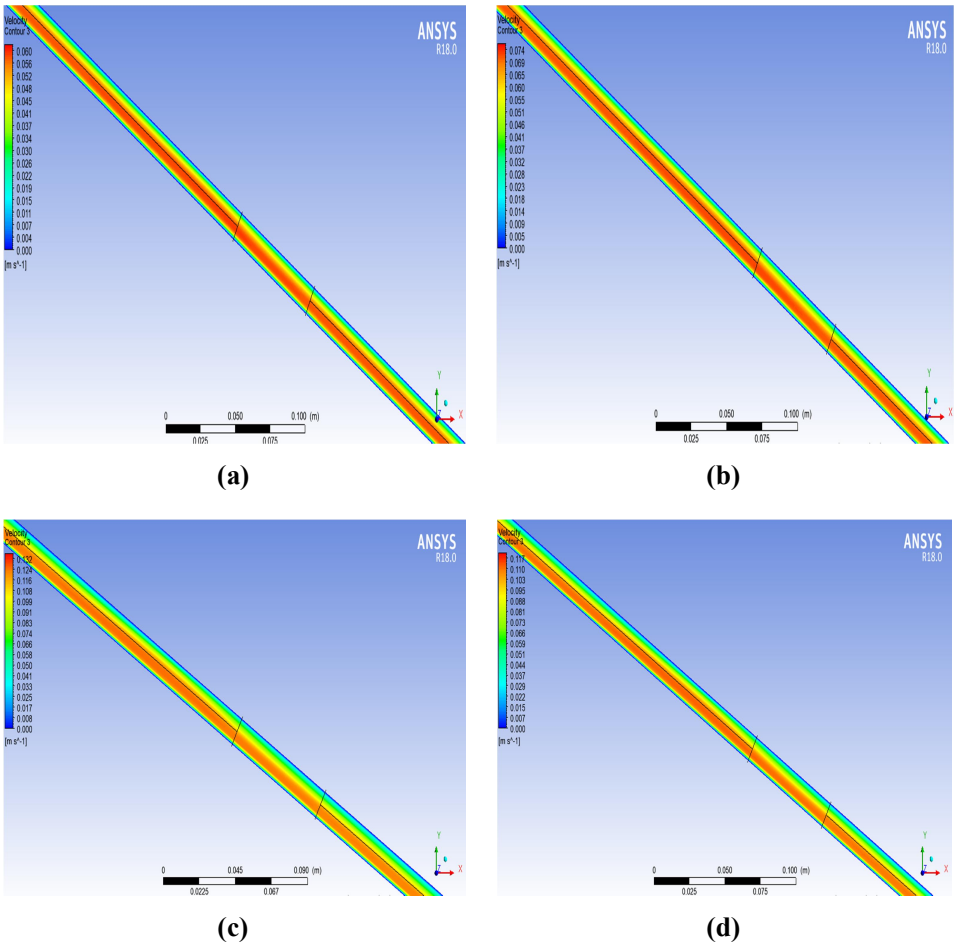

Fig. 10: Water Velocity Distribution Along the Absorber Subjected to Electromagnetic Field 3240 Gauss a) 9:00 Am b) 11:00 AM c) 13:00 PM d)15:00 PM

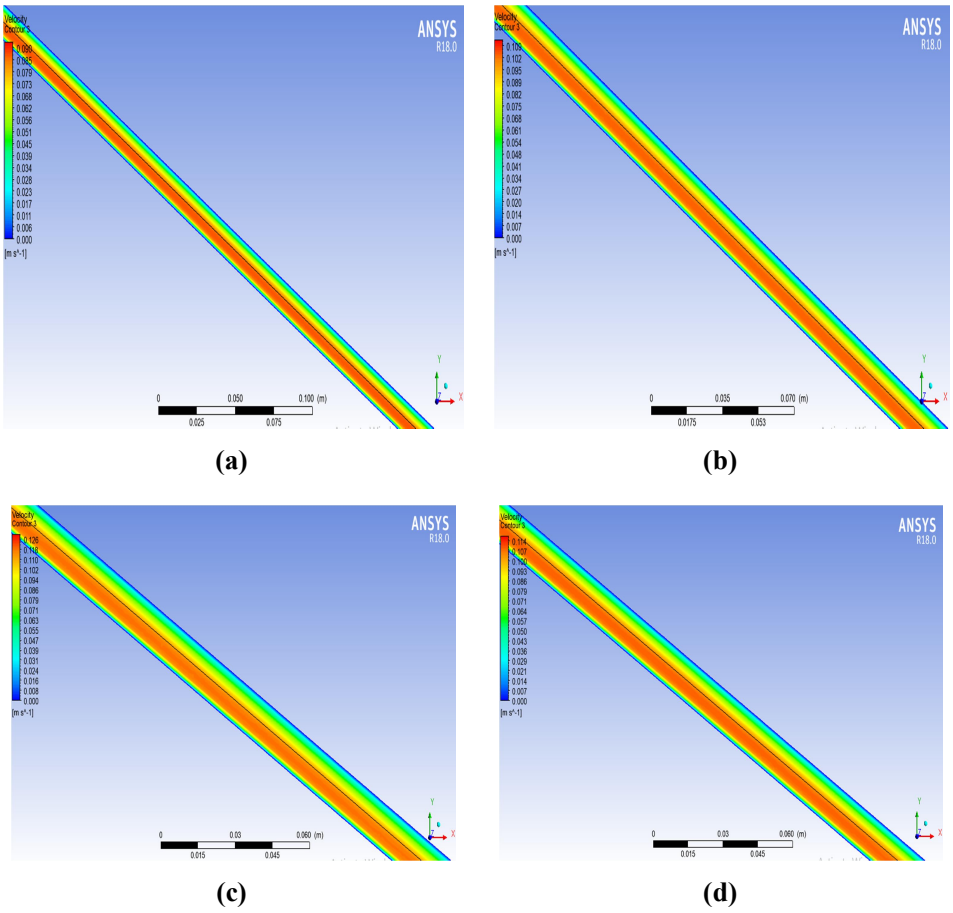

Fig. 11: Ferrofluid(φ =0.3%) Velocity Distribution Along the Absorber no Subjected to Electromagnetic Field a)9:00 Am b)11:00 AM c)13:00 PM d)15:00 PM

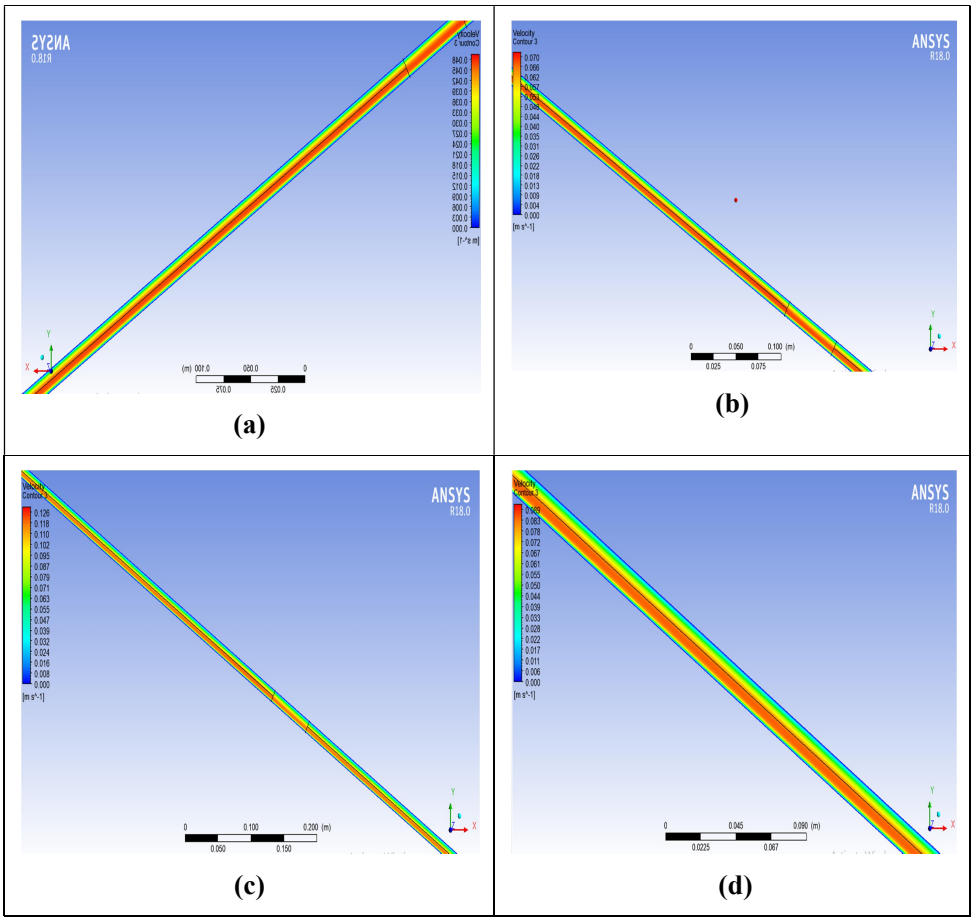

Fig. 12: Ferrofluid(φ =0.3%) Velocity Distribution Along the Absorber Subjected to Electromagnetic Field3420 Gauss a)9:00 Am b)11:00 AM c)13:00 PM d)15:00 PM.

IV. Conclusions

This study is carried out to investigate the effect used magnetic nanofluid flow with and without electromagnetic field. The nanofluid containing oxide metal nanoparticles has a magnetic behavior in water.

The heat transfer enhanced with increasing nanoparticle concentration (0.3, 0.6, and 0.9 %). The use of electromagnetic field further enhances the heat transfer, the Heat transfer enhanced with increasing magnetic intensity. If water is used, the effect of the electromagnetic field is very little or no noticeable. The ferrofluid (Fe_3O_4+water) shows more heat transfer enhancement. The addition of nanoparticles makes the properties of heat transfer characteristics higher and better than base fluid (water).

References

I Abu-Nada, E, "Application of nanofluids for heat transfer enhancement of separated flows encountered in a backward-facing step", International Journal of Heat and Fluid Flow.; 242-24,. (2008).

II Aminfar H., Mohammad P. M., Mohseni F., "Two-phase mixture model simulation of the hydro-thermal behavior of an electrical conductive ferrofluid in the presence of magnetic fields", Journal Magn. Magn. Mater.; 324, 830-842, (2012).

III Duffie J A., Beckman W A., "Solar energy thermal processes", in, University of Wisconsin- Madison, Solar Energy Laboratory, Madison, WI, (1974).

IV Hussein A. K., Ashorynejad H. R., Sheikholeslami M., Sivasankaran S., "Lattice Boltzmann simulation of natural convection heat transfer in an open enclosure filled with Cu–water nanofluid in a presence of magnetic field", Nucl. Eng. Des.; 268, 10-17, (2014).

V Maiga S. E. B., Cong T. N., "Heat transfer enhancement in turbulent tube flow using Al_2O_3 nanoparticle suspension", International Journal of Numerical Methods for Heat and Fluid Flow.; 275-29, (2006).

VI Mohsen S., Mofid G. B., Ellahibc A. Z., "Simulation of MHD CuO–water nanofluid flow and convective heat transfer considering Lorentz forces", Journal of Magnetism and Magnetic Materials.; 369, 69-80, (2014).

VII Nagarajan P K., Subramani J., Suyambazhahan S., Sathyamurthy R., "Nanofluids for solar collector applications: A Review", Energy Procedia; 61: 2416 – 2434, (2014).

VIII Sheikhzadeh G A, Sebdani1 M S, Mahmoodi M, Elham S, Hashemi S E. "Effect of a Magnetic Field on Mixed Convection of a Nanofluid in a Square Cavity", Journal of Magnetics.;18, 321-325, (2012).

IX Titan C., Morshed A. M., Jamil A.K., "Nanoparticle enhanced ionic liquids (NEILS) as working fluid for the next generation solar collector", Procedia Engineering, 5th BSME International Conference on thermal engineering.; 56, 631-636, (2013).

X Tyagi H., Phelan P., Prasher R., "Predicted Efficiency of a Low-Temperature Nanofluid–Based Direct Absorption Solar Collector", Journal of Solar Energy Eng. 131, 041004, (2009).

XI Zhang Z., Gu H., Fujii M., "Effective thermal conductivity and thermal diffusivity of nanofluids containing spherical and cylindrical nanoparticles", Exp. Therm. Fluid Sci.; 31, 5593-5599, (2007).